JOURNAL OF APPLIED PHYSICS VOLUME 89, NUMBER 2 15 JANUARY 2001

Nonspecular x-ray reflectivity study of roughness scaling in Si/Mo multilayers

J. M. Freitag[a] and B. M. Clemens
Department of Materials Science and Engineering, Stanford University, Stanford, California 94305-2205

(Received 10 July 2000; accepted for publication 17 October 2000)

The interfacial roughness and lateral correlation length of a series of Si/Mo multilayers with bilayer period 69 Å and number of bilayers ranging from 5 to 40 have been characterized by diffuse x-ray scattering. Superlattice peaks are preserved in offset radial scans indicating a high degree of conformality in the roughness. The lateral correlation length ξ increases with total film thickness h as $\xi \sim h^{0.55}$; however, the magnitude of the roughness is approximately 2 Å for all film thicknesses, in disagreement with scaling laws for self-affine growing surfaces. This observation suggests that interfaces retard the evolution of high-frequency roughness while replicating longer wavelength roughness from one layer to the next © *2001 American Institute of Physics.*
[DOI: 10.1063/1.1332095]

I. INTRODUCTION

The continued shrinking of microelectronic device size, which is nearing the diffraction limit of conventional photolithography systems, necessitates the development of optical imaging systems operating in the soft x ray, or extreme ultraviolet (EUV), regime. These next-generation EUV lithography systems will require reflective optics coated with multilayer films. The Si/Mo multilayer coating is a leading candidate for this purpose due to the large electron contrast and smooth layering of its constituents. Yet, the nonideal nature of the interfaces limits the reflectivity of these multilayer coatings. Imperfections arise during the growth process in part due to intermixing and reaction of Mo and Si. In general, roughness is defined as the standard deviation of the interface height and leads to nonspecular scattering. This nonspecular, diffuse, scattering is problematic for EUV imaging systems because it decreases the useful throughput of the system and produces a background halo that reduces the contrast of the image.[1] In this paper we will describe a series of experiments using x-ray diffraction to characterize the evolution of roughness and lateral roughness correlations in Si/Mo multilayers. The paper is organized as follows: Sec. II presents the theoretical background for scattering from a single rough surface and its extension to multilayers. We describe the experiment in Sec. III, followed by results and discussion in Sec. IV. We begin though by introducing some scaling concepts of surface growth theory.

Surface morphology of growing films commonly shows fractal behavior, i.e., film roughness appears similar over many orders of magnification. Fractal objects that are preserved under an isotropic scale transformation are called self-similar; typically, surfaces must be rescaled anisotropically and are known as self-affine. However, film morphology is not self-affine at all length scales: at small enough magnification a growing film will appear smooth. Consider a growing two-dimensional surface characterized by the height function $h(\mathbf{r},t)$ at time t. According to the Family–Vicsek scaling theory,[2] the time evolution of the interface width is described by the relation

$$w_L \sim L^{\alpha} f\left(\frac{t}{L^z}\right), \tag{1}$$

where $f(u)$ is the scaling function which has the following form:

$$f(u) \sim \begin{cases} u^{\beta} & [u \ll 1] \\ \text{const.} & [u \gg 1] \end{cases}, \tag{2}$$

and where L is the length scale over which roughness is measured, α and β are the static and dynamic scaling exponents, respectively, and z is α/β.[3] In the limiting cases, Eq. (1) reduces to

$$w_L \sim t^{\beta} \quad [t/L^z \ll 1], \tag{3}$$

and to

$$w_L \sim L^{\alpha} \quad [t/L^z \gg 1]. \tag{4}$$

For a self-affine surface, a plot of w_L vs L on a log–log scale yields a straight line with slope $0<\alpha<1$; for a self-similar surface, $\alpha=1$. However, above some critical length ξ, roughness saturates to the root mean square (rms) roughness $\sigma \equiv [\langle h(\mathbf{r})^2 \rangle]^{1/2}$. This critical length for scaling can be viewed as the lateral correlation of a self-affine surface, which itself scales according to the Family–Vicsek relation. At the beginning of growth, $\xi=0$ because the entire surface is uncorrelated. During growth ξ increases with time. In a finite system though, ξ cannot grow indefinitely. When it reaches the size of the system L, the entire interface becomes correlated. At this point, roughness saturates and we find

$$\xi \sim L \quad [t/L^z \gg 1]. \tag{5}$$

This saturation occurs, according to Eqs. (1) and (2), when $t \sim L^z$. Replacing L with ξ, we obtain the scaling relation for the lateral correlation length

$$\xi \sim t^{\beta/\alpha}. \tag{6}$$

[a]Electronic mail: jfreitag@us.ibm.com

 © 2001 American Institute of Physics

Downloaded 10 Sep 2002 to 148.6.178.13. Redistribution subject to AIP license or copyright, see http://ojps.aip.org/japo/japcr.jsp

We also note that the scaling relationships involving time can be recast with film thickness when the film is deposited at a constant rate. For instance, interface width therefore scales as film thickness to the power β.

II. SCATTERING THEORY

A. Scattering of x rays from a single rough surface

The effect of roughness on the intensity of specular reflections is well-known. For a single rough surface with rms roughness σ, the specular reflectivity I_{spec} is attenuated by an exponential

$$I_{\text{spec}}=I_0 \exp(-q_z^2\sigma^2), \tag{7}$$

where I_0 is the specular reflectivity of a perfect crystal and q_z is the out-of-plane momentum transfer vector. The derivation of this result is analogous to the Debye–Waller effect for a Gaussian distribution of thermally displaced atoms.[4] In the case of a rough surface, to derive Eq. (7), we still require a Gaussian distribution of surface heights but we assume the disorder is frozen in. The intensity that is lost in the specular direction is diffusely scattered by the arbitrarily rough surface; however, calculating the shape of this diffuse scattering is a complex problem. Sinha *et al.*[5] have developed a scattering theory for nonideal surfaces. In this model, the z direction is the average film normal and the surface heights are described by a single-valued function, $h=z(x,y)$, which is a Gaussian random variable. Starting from the first-order Born approximation of the differential cross section for scattering

$$\frac{d\sigma}{d\Omega}=N^2b^2\int_V d\mathbf{r}\int_V d\mathbf{r}'\, e^{-i\mathbf{q}\cdot(\mathbf{r}-\mathbf{r}')}, \tag{8}$$

where b, for x rays, is the electronic scattering length (e^2/mc^2) and N is the electron number density, it can be shown that the scattered intensity per unit area is

$$I(\mathbf{q})=I_0\exp(-q_z^2\sigma^2)/q_z^2\int\int dx\,dy\,\exp[q_z^2C(x,y)] \times\exp[-i(q_xx+q_yy)]. \tag{9}$$

In this expression the height–height correlation function $C(x,y)$, defined as

$$C(x,y)=\langle z(x-x',y-y')z(x,y)\rangle, \tag{10}$$

specifies roughness and provides quantitative information about both the height variations and the lateral correlation. A simple form of the correlation function for a self-affine surface with a cutoff length ξ, proposed by Sinha, is

$$C(x,y)=C(R)=\sigma^2e^{-(R/\xi)^{2\alpha}}, \tag{11}$$

where the exponent α is the roughness exponent introduced in the scaling relation of Eq. (1). Computer simulations of surface dynamics with different roughness exponent α give manifestly different interfaces: small values of α produce jagged surfaces, while values of α approaching 1 appear smooth. In Eq. (11), we assume that roughness is isotropic so that C is only a function of the magnitude of $R=(x^2+y^2)^{1/2}$ for all points on the surface with coordinates separated by (x,y). Alternate forms of the correlation function that obey the scaling requirement have been proposed.[6] In this study however, we defer to the most commonly used correlation function given in Eq. (11).

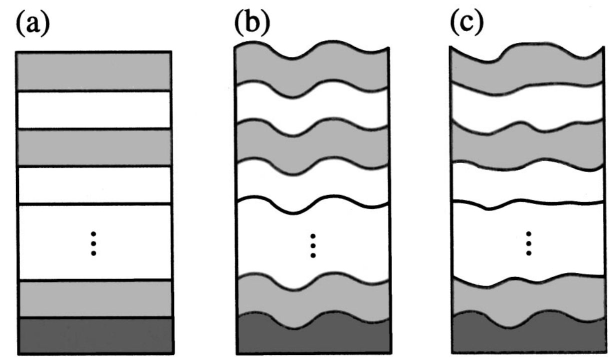

FIG. 1. Schematics of multilayer structures: (a) ''ideal'' multilayer, (b) conformal roughness, (c) uncorrelated layer roughness.

We insert Eq. (11) into Eq. (9) and simplify the equation to a one-dimensional problem by integrating both sides over y. In practice, this integration is realised by detecting the scattered intensity with a sufficiently long slit. For $\alpha=1/2$ or 1, the equation can be solved analytically; however, we must perform a numerical integration for arbitrary α. With $\alpha=1/2$, the correlation function is

$$C(R)=\sigma^2\exp(-R/\xi). \tag{12}$$

The term $\exp[q_z^2C(x,0)]$ in Eq. (9) can be expanded and each term Fourier transformed analytically. The integration yields

$$I(q_x,q_z)=2\pi I_0(e^{-q_z^2\sigma^2})/q_z^2 \times\left[2\pi\delta(q_x)+\sum_{m=1}^{\infty}\frac{2\xi(q_z^2\sigma^2)^m}{m(m!)}\times\frac{1}{1+q_x^2\xi^2/m^2}\right] \tag{13}$$

which is a sum of a delta function (the specular reflection being convolved, in practice, with a finite detector resolution) and a diffuse term. The diffuse term is a sum of Lorentzians whose width is inversely related to the correlation length ξ.

B. Multilayer reflectivity

Up to this point we have only considered scattering from a single rough surface. In multilayers, the incident field scatters at each rough interface. Therefore, calculation of the scattering amplitude requires knowledge of the roughness correlation function for each interface and their cross-correlations,

$$C_{ij}=\langle h_i(\mathbf{r})h_j(\mathbf{r}')\rangle, \tag{14}$$

where i,j are interface labels. Figure 1 schematizes extreme roughness distributions within a multilayer: (a) no roughness, (b) each layer conformally replicating the underlying roughness, and (c) uncorrelated roughness from layer to layer. The term ''correlated'' should not be confused with the lateral correlation length described previously. In the present context it refers to how the profiles of consecutive interfaces map onto one another in the multilayer. For the

Downloaded 10 Sep 2002 to 148.6.178.13. Redistribution subject to AIP license or copyright, see http://ojps.aip.org/japo/japcr.jsp

case of uncorrelated roughness, i.e., $C_{ij}=0$ for $i\neq j$, the scattered intensity from each interface adds incoherently and we measure the average of the scattering cross sections of the top N interfaces, where N depends on the penetration depth of the x rays.[7] Similarly, for perfect conformal roughness, we measure N statistically equivalent interfaces.

It is well-known that the specular scattered fields of multiple interfaces add coherently and produce peaks at the Bragg condition ($q_z=m2\pi/\Lambda$, where Λ is the bilayer period) whose amplitudes are determined by the Fourier coefficients of the composition modulation.[8] Rough multilayers can exhibit similar peaks in the diffuse scattering. These so-called *Bragg sheets* arise from interfacial defects that are to some degree replicated from interface to interface.[9] Payne *et al.* show that conformal roughness is indeed a necessary condition for coherent nonspecular scattering.[10] In practice, multilayer interfaces are only partially correlated. In this case, the interface can be described by decomposing its profile function into a totally correlated component and an uncorrelated component representing the intrinsic roughness. The correlated component scatters intensity in the Bragg sheets, whereas the intensity between two sheets results from uncorrelated fluctuations.[7]

We will see shortly that the Si/Mo multilayers presented in this paper exhibit strong coherent scattering features including finite thickness oscillations in the diffuse spectra. Such features evidence a high degree of conformality in the multilayer structure. In this regard, the scattering theory for a single rough layer developed in the previous section can be justifiably applied to the case of the Si/Mo multilayers presented here. Indeed, for perfect, conformally rough multilayers, the scattered intensity is a convolution of the scattered intensity of a single rough layer with the modulation factor associated with the superlattice structure.

III. EXPERIMENT

A. Multilayer deposition

Si/Mo multilayers were deposited by dc magnetron sputtering in a system with a base pressure of $\leqslant 5\times10^{-9}$ Torr and with an Ar sputtering pressure of 1.5 mT. The nominal deposition rate measured with a crystal rate monitor without tooling factors was 1 Å/s. All depositions were, nominally, at room temperature. A small temperature increase of less than 4° had previously been measured under similar deposition conditions. The individual layer thicknesses were controlled with mechanical shutters over the elemental sputtering targets.

To study the effect of film thickness on roughness correlations, we deposited a series of Si/Mo multilayers with nominal bilayer period Λ of 69 Å, $\Gamma=0.4$, and number of bilayers $N=5.5$, 10.5, 20.5, and 40.5, i.e., each stack began and ended with Si. Γ refers here to the volume fraction of Mo in the multilayer. We also deposited a series of samples with $\Lambda=69$ Å, $N=20.5$, and Γ varying from 0.2 to 0.8. The Si(100) wafers used as substrates were cleaned with acetone and ethanol. The native oxide was not stripped. We achieved a bilayer period as close as possible to the desired 69 Å with the appropriate Γ using x-ray diffraction to determine the correct deposition times for Mo and Si. The technique, which takes into account the intermixing and associated contraction of the bilayer period, is described elsewhere.[11]

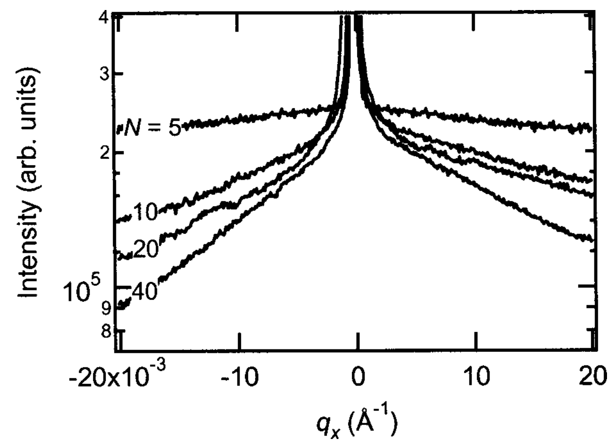

FIG. 2. Transverse k-scans along the seventh order Bragg peak in Si/Mo multilayers with N bilayers, where N, from top to bottom, is 5, 10, 20, and 40.

B. Synchrotron x-ray diffraction

All small-angle reflectivity measurements were performed on the focused bending magnet powder diffraction beamline, BL 2-1, at the Stanford Synchrotron Radiation Laboratory (SSRL). X rays of energy 8051 eV, monochromated by a Si(111) double-crystal, were focused to a spot size of 1.0×2.0 mm. The diffractometer is designed around two large concentric Huber goniometers. Four types of scans were conducted: specular θ–2θ reflectivity scans, offset scans with $\omega=\theta-2\theta/2<0$ for off-specular reflectivity, transverse θ (or ω) rocking scans, and, more useful, transverse k-scans in which only the transverse component of the scattering vector varies.

IV. RESULTS AND DISCUSSION

Before embarking on a detailed analysis using the theory presented in Sec. II, we note that an important conclusion can be drawn immediately by qualitative inspection of the diffuse scattering data. Consider in Fig. 2 the transverse k-scans about the seventh order Bragg peak for a series of Si/Mo multilayers with increasing number of bilayers N. One observes quite clearly that the width of the diffuse scattering decreases with increasing N, indicating that the lateral length-scale of the roughness is increasing. As expected, the scattered intensity, Eq. (13), based on a self-affine roughness model, also predicts that the width of the diffuse scattering is inversely proportional to the correlation length. In the following analysis, we attempt to estimate the correlation length using this self-affine model. We begin by presenting specular and offset $(\theta,2\theta)$ scans to establish the conformal nature of the roughness in Si/Mo multilayers.

A. Specular and diffuse reflectivity

An example of the small-angle specular and off-specular reflectivities for a Si/Mo multilayer with 20 bilayers is shown in Fig. 3. The large number of superlattice Bragg

Downloaded 10 Sep 2002 to 148.6.178.13. Redistribution subject to AIP license or copyright, see http://ojps.aip.org/japo/japcr.jsp

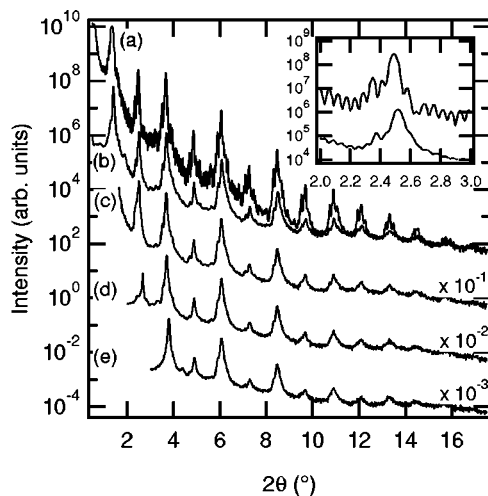

FIG. 3. Reflectivity spectra for a Si/Mo multilayer with 20 bilayers and bilayer period $\Lambda=73.0$ Å. From top to bottom, the θ–2θ scans are (a) specular reflectivity ($\omega=0$), (b) off-specular reflectivity with $\omega=0.25°$, (c) $\omega=0.5°$, (d) $\omega=1.0°$, and (e) $\omega=1.5°$. The inset is a detail of the second Bragg peak showing finite thickness oscillations in both the specular and off-specular ($\omega=0.25°$) spectra. For clarity, off-specular scans are vertically offset as indicated in the figure.

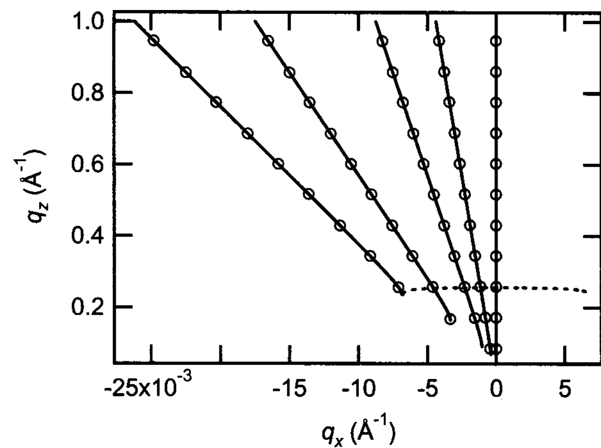

FIG. 4. Reciprocal space map showing the paths of the scans from Fig. 3 as solid lines. The circles indicate the positions of the superlattice Bragg peaks. The dotted line is the path a θ rocking curve about the third superlattice peak traces through reciprocal space.

peaks that extend above 16° in 2θ ($q_z>1.13$ Å^{-1}) and high-reflectivity indicate very smooth layering. A sample with 40 bilayers grown under the same conditions exhibited a peak normal-incidence reflectivity of 65.7% at 136 Å wavelength radiation. Qualitatively, from observation of the extinction of higher-order Bragg peaks, the total roughness appears independent of the number of bilayers. No theoretical modelling was undertaken in this study, mainly due to the difficulty in extracting a unique set of structural parameters from fitting to the data. Indeed, Mo and Si readily intermix at the interfaces forming a compound with a stoichiometry close to $MoSi_2$.[12] The resulting interlayers are reported to be asymmetric with the Mo on Si interlayer roughly twice as thick as Si on Mo.[13] The complexity of this structure therefore necessitates a large number of independent fitting parameters to adequately simulate it. Instead, we will quantitatively deduce the correlated roughness from the *diffuse* scattering.

Offset (θ,2θ) scans are also depicted in Fig. 3 while Fig. 4 shows the paths through reciprocal space, as solid lines, that these offset scans trace. The circle symbols in the latter figure indicate the positions of the superlattice Bragg peaks for each scan. The presence in the diffuse spectra of these peaks due to coherent scattering, as well as finite thickness oscillations visible in the inset close-up of Fig. 3, clearly indicates a high degree of conformality and interface roughness replication. Recall that uncorrelated interface roughness would generate none of the coherent diffuse scattering evident in Fig. 3.

Transverse θ rocking scans provide information on the lateral length scale or in-plane correlation length ξ of the film. An example of such a rocking scan about the third superlattice peak for the previous 20 bilayer multilayer is shown in Fig. 5. Several geometrical factors may affect the shape of these rocking curves. First, the footprint of the beam on the sample varies with the incident angle θ_i as $s_y/\sin(\theta_i)$, where s_y is the size of the beam defining slit. The second factor is due to the increased absorption from the increased path length through the multilayer at low incident or exit angles. A correction factor for an N-bilayer mirror, estimated using kinematic diffraction theory,[14] was applied to the rocking curve depicted in Fig. 5. A third factor, however, is more difficult to estimate. It arises from the geometry of the path of a rocking curve through reciprocal space. As shown in Fig. 4, because the length of the scattering vector is constant in a rocking scan, its path (dotted line) deviates from the q_x, q_y plane at the superlattice diffraction condition q_z when $|\omega|>0$. The intensity of a rocking scan will consequently fall off with increasing $|\omega|$. For this reason we will consider in our subsequent analysis only true transverse scans in which the z-component of the scattering vector is kept constant and the diffraction condition is satisfied for all values of q_x.

Of interest to note, rocking scans display satellite peaks at off-specular angles. The strongest of these peaks at the tails of the rocking curve in Fig. 5 occur when the incident or exit angle satisfies the Bragg condition. The smaller peaks

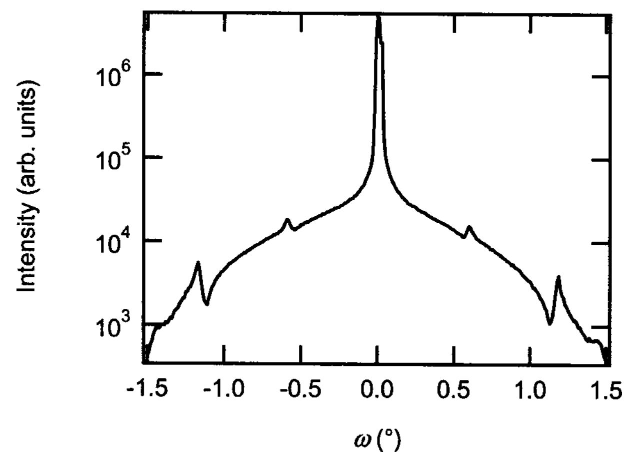

FIG. 5. θ rocking scan about the third superlattice peak in a 20 bilayer Si/Mo multilayer.

Downloaded 10 Sep 2002 to 148.6.178.13. Redistribution subject to AIP license or copyright, see http://ojps.aip.org/japo/japcr.jsp

TABLE I. Roughness σ and effective in-plane correlation length ξ for Si/Mo multilayers with N bilayers, nominal Mo thickness ratio $\Gamma = t_{Mo}/(t_{Mo}+t_{Si})$, and measured bilayer period Λ.

N	Γ	Λ (Å)	σ (Å)	ξ (Å)
5	0.4	74.8	2.5	19
10	0.4	77.5	2.6	24
20	0.4	73.0	2.2	33
40	0.4	70.8	2.1	52
20	0.2	68.0	2.4	31
20	0.6	67.4	3.2	51
20	0.8	69.3	4.1	111

appearing at intermediate angles corresponding to the second order Bragg reflection arise from double diffraction.[14] Furthermore, Yoneda wings become manifest when the incident or exit angle equals the critical angle for total external reflection.[15] None of these effects are accounted for in the fitting procedures used in this paper which we discuss in the following section.

B. Fitting procedure for transverse scans

In Sec. II A we developed an expression, Eq. (13), for the diffuse scattering of x rays in the Born approximation using the Sinha correlation function, Eq. (11), and $\alpha=1/2$. The validity of this choice of α will be discussed shortly. Our diffuse spectra consist of transverse k-scans along the Bragg sheets of each sample up to the eleventh order. We model these profiles using Eq. (13) and vary the in-plane correlation length ξ and roughness σ to obtain a best fit. Careful attention is paid to the convergence of the sum of Lorentzians in Eq. (13). For small product $q_z\sigma$, the sum converges rapidly. With $q_z\sigma\sim 2$ up to 70 terms are required to achieve numerical convergence. For a given surface roughness and a limited number of terms in the fitting procedure, this imposes an upper limit on q_z and the number of Bragg sheets that can be included in the analysis.

C. Correlated roughness results

Table I summarizes the results of the diffuse scattering fitting. The value quoted for roughness σ represents only the correlated roughness since it is extracted from the diffuse scattering intensity of a single layer applied to multilayers under the assumption of perfect conformal roughness. In general, the total roughness will have contributions from vertically uncorrelated roughness,

$$\sigma_{tot}=\sqrt{\sigma_c^2+\sigma_u^2}, \tag{15}$$

where σ_c and σ_u are the correlated and uncorrelated roughness, respectively. As justified earlier, the roughness of the mirrors in this study appear to be highly conformal. Therefore we may presume that the correlated roughness will dominate the uncorrelated contribution.

Up to this point, Eq. (13) has been used exclusively to model the diffuse scattering without justification of the choice of the scaling coefficient $\alpha=1/2$. This assumption was necessary to analytically solve the general expression for the total scattering, Eq. (9). Figure 6 shows an example of a transverse k-scan along the fourth-order superlattice Bragg sheet ($q_z=0.3718\,\text{Å}^{-1}$) for a 20-bilayer Si/Mo multilayer with $\Gamma=0.8$. Correction factors for absorption at low incident or exit angles as well as the larger beam footprint at low incident angle have been applied. In contrast to θ rocking curves, no correction is necessary to account for any divergence from the x,y plane at the Bragg condition since the length of the scattering vector is automatically adjusted during the scan with q_z held constant. The solid line in Fig. 6(a) is a fit obtained by direct numerical integration of the total scattering, Eq. (9), with the correlation function of Eq. (11) and $\alpha=1/2$. The fit parameters are consistent with the results obtained using the analytical expression, Eq. (13). Figure 6(b) is a close-up of the high-q_x tail of the diffuse scattering showing best fits with three different values of α. Fitting the diffuse scattering with smaller values of α, i.e., more jagged surfaces, requires in general a smaller correlation length. The lateral correlation length decreases from 216 Å to 22 Å for α ranging from 0.9 to 0.25. The figure clearly shows that the fit using a scaling coefficient of 1/2 best describes the shape of the diffuse scattering. The fitting procedure described in the previous section is therefore justified.

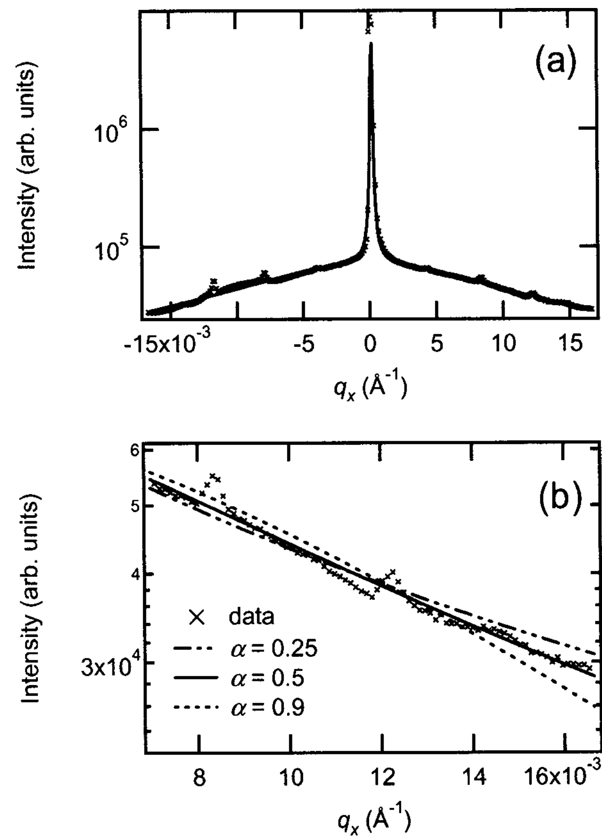

FIG. 6. (a) Transverse k-scan for a Si/Mo multilayer with 20 bilayers and $\Gamma=0.8$. The solid line is the best fit obtained by numerically integrating the general expression for the scattered intensity with a roughness coefficient $\alpha=0.5$. (b) Close-up of high-q_x tail showing the effect on the shape of a best fit using different values of α. The best-fit parameters for each α were: $\alpha=0.25$, $\xi=22$ Å, $\sigma=1.8$ Å; $\alpha=0.5$, $\xi=111$ Å, $\sigma=3.6$ Å; $\alpha=0.9$, $\xi=216$ Å, $\sigma=5.4$ Å.

D. Roughness scaling

Finally, we discuss the scaling laws for roughness presented earlier and upon which our particular choice of rough-

Downloaded 10 Sep 2002 to 148.6.178.13. Redistribution subject to AIP license or copyright, see http://ojps.aip.org/japo/japcr.jsp

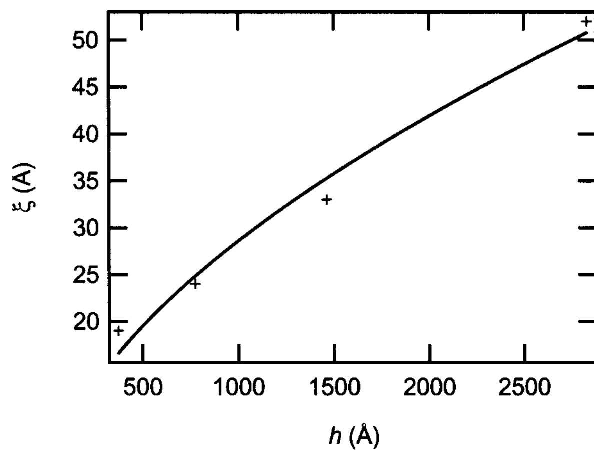

FIG. 7. Lateral correlation length ξ as a function of total thickness for a series of Si/Mo multilayers with $\Gamma=0.4$. The solid line is a power-law fit with the scaling parameter $1/z=0.55$.

ness correlation function depended. Recall from Eq. (6) that the time evolution of the lateral correlation length should follow a power-law scaling relationship $\xi=\xi_0 t^{1/z}$, where ξ_0 is the correlation length for a given time t_0. For a constant deposition rate, time can be replaced by thickness. Figure 7 shows the evolution of correlation length as a function of the total thickness $h=N\Lambda$ for the series of multilayers with $\Gamma=0.4$ and number of bilayers N ranging from 5 to 40. The solid line is a power-law fit with a scaling coefficient $1/z=0.55$. Admittedly, the small data set presented in this graph prevents drawing any strong conclusions. Nevertheless, given $\alpha=1/2$ and $z=\alpha/\beta$, our result implies a dynamic scaling coefficient $\beta=0.28$. According to the scaling law, Eq. (3), roughness is expected to increase with thickness to the power β; however, Table I shows that roughness appears to be independent of thickness within experimental error. Other studies report similar findings for W/C multilayers.[16] The authors speculated there that the interfaces suppress the increase in roughness by providing periodic ''restarting layers'' during growth. However, the mere presence of the interfaces is insufficient to completely explain the roughening process. For Si/Mo multilayers, both the lateral correlation length and the roughness increase with Γ, as can be seen in Table I. The Si layers, which are amorphous, appear to smooth the cumulative roughness intrinsic to polycrystalline Mo growth.

In contrast, Stearns *et al.*[1] report that roughness doubles from 0.9 Å at the substrate to 1.8 Å at the top surface in a 40-bilayer Mo/Si multilayer. Their observation is based on integrating the power spectral density (PSD) function (which is the Fourier transform of the autocorrelation function) obtained by atomic force microscopy (AFM) over the entire frequency range. Roughness at each layer is inferred from the PSDs of the bare substrate and top multilayer surface using a linear growth model to describe the growth dynamics. It is possible that the correlated roughness reported in the present paper greatly underestimates the total roughness which includes an uncorrelated contribution; uncorrelated roughness would, ostensibly, increase during growth. This seems unlikely though based upon the observation of coherent scattering effects in the diffuse spectra and on the high-reflectivity exhibited by the multilayers. Larger total roughness would suppress the high-order Bragg reflections that we observe. Furthermore, AFM measurements give rms roughness in agreement with the values reported in Table I.

A question that remains unanswered is how roughness can be conformal while the in-plane correlation length increases. One possible reason, suggested by Savage *et al.*,[16] is that the interfaces act to preferentially smooth the high-frequency components of roughness. The long wavelength components, on the other hand, are replicated through the multilayer stack and give rise to coherent diffuse scattering. Although the roughness values listed in Table I are, within experimental error, very similar, there appears to be a trend toward slightly smaller correlated roughness for samples with more bilayers. The multilayers remain, nevertheless, highly conformal because growth attenuates only high-frequency roughness. The spatial filtering hypothesis is plausible in the context of surface growth models which incorporate a surface relaxation term since relaxation tends to preferentially flatten sharp surface features (see Ref. 17, for instance). Under such conditions, large surface defects would be propagated from the substrate to the top of the film degrading the reflective optics and masks used in extreme ultraviolet lithography systems.

V. CONCLUSIONS

The evolution of roughness and roughness correlations were measured in sputtered Si/Mo multilayers by synchrotron x-ray diffraction. An expression for the total scattered intensity from a self-affine rough surface was presented. This expression was extended to multilayers with correlated, conformal roughness. The conformal nature of the roughness in Si/Mo multilayers was confirmed by the presence of coherent scattering in the diffuse spectra. A static scaling coefficient $\alpha=1/2$ for roughness best describes this diffuse spectra. By fitting the shape and intensity of the diffuse spectra, we extracted the roughness and in-plane correlation lengths. A series of multilayers grown with the same nominal bilayer structure and number of bilayers varying from 5 to 40 demonstrates that the correlation length increases, scaling with a coefficient $\beta/\alpha=0.55$. The roughness of the multilayers, however, is independent of thickness, contrary to the scaling law prediction. This discrepancy is ascribed to the smoothing effect of the amorphous interfaces. Conformal layer-to-layer roughness replication is retained assuming that interfaces preferentially flatten only the high-frequency components of roughness.

ACKNOWLEDGMENTS

One of the authors (J.M.F.) gratefully acknowledges support from the Stanford Graduate Fellowship program. Synchrotron work was done at SSRL, which is operated by the Department of Energy, Office of Basic Energy Sciences.

[1] D. G. Stearns, D. P. Gaines, D. W. Sweeney, and E. M. Gullikson, J. Appl. Phys. **84**, 1003 (1998).
[2] F. Family and T. Vicsek, J. Phys. A **18**, 75 (1985).
[3] W. M. Tong *et al.*, Phys. Rev. Lett. **72**, 3374 (1994).

Downloaded 10 Sep 2002 to 148.6.178.13. Redistribution subject to AIP license or copyright, see http://ojps.aip.org/japo/japcr.jsp

[4] R. W. James, *The Optical Principles of the Diffraction of X Rays* (Ox Bow Press, Woodbridge, 1982).
[5] S. K. Sinha, E. B. Sirota, and S. Garoff, Phys. Rev. B **38**, 2297 (1988).
[6] G. Palasantzas and J. Krim, Phys. Rev. B **48**, 2873 (1993).
[7] T. Salditt *et al.*, Phys. Rev. B **51**, 5617 (1995).
[8] J. M. Cowley, *Diffraction Physics* (North–Holland, Amsterdam, 1984).
[9] J. M. Elson, J. P. Rahn, and J. M. Bennett, Appl. Opt. **19**, 669 (1980).
[10] A. P. Payne and B. M. Clemens, Phys. Rev. B **47**, 2289 (1993).
[11] J. M. Freitag and B. M. Clemens, Proc. Mater. Res. Soc. **562**, 177 (1999).
[12] D. G. Stearns, R. S. Rosen, and S. P. Vernon, Proc. SPIE **1547**, 2 (1992).
[13] K. Holloway, D. K. Ba, and R. Sinclair, J. Appl. Phys. **65**, 474 (1989).
[14] D. E. Savage *et al.*, J. Appl. Phys. **69**, 1411 (1991).
[15] Y. Yoneda, Phys. Rev. **131**, 2010 (1963).
[16] D. E. Savage, N. Schimke, Y. H. Phang, and M. G. Lagally, J. Appl. Phys. **71**, 3283 (1992).
[17] A.-L. Barabási and H. E. Stanley, *Fractal Concepts in Surface Growth* (Cambridge University Press, Cambridge, 1995).

Downloaded 10 Sep 2002 to 148.6.178.13. Redistribution subject to AIP license or copyright, see http://ojps.aip.org/japo/japcr.jsp